Structural Implications of the Elliptical Form of Small-Angle Reflections in Oriented Semicrystalline Polymers

N. S. Murthy,*,† D. T. Grubb,‡ and K. Zero†

Research and Technology, AlliedSignal Inc., P.O. Box 1021, Morristown, New Jersey 07962, and Department of Materials Science and Engineering, Cornell University, Ithaca, New York 14853

Received July 15, 1999; Revised Manuscript Received November 11, 1999

ABSTRACT: The intensity maxima of lamellar reflections in small-angle scattering patterns from uniaxially oriented polymers such as fibers do not generally fall on a straight layer line or on a circular arc. The shape of the reflection can be analyzed by measuring the periodicity L_ϕ of the lamellar planes as a function of the angle ϕ between the reflection and z. L_ϕ is measured parallel to the fiber axis z. The data give a straight line in a plot of L_ϕ^2 vs $\tan^2 \phi$. This shows that the reflection is elliptical and provides a basis for fitting small-angle patterns in an elliptical coordinate system using few parameters. Further analysis of patterns that extend to large values of ϕ shows that an elliptical fit is not merely a convenience; it is also the best fit. Many possible structures could cause the lamellar reflection to lie on a curve, but few models predict an ellipse. The simplest is affine deformation of the lamellar structure. Recognizing that a single lamellar population will give reflections of an elliptical form allows populations of lamellae to be distinguished even when the reflections overlap strongly, with long spacings L_M different by only 2−8%. This permits a greater understanding of the processes of fiber drawing and annealing.

Introduction

The crystalline domains in many semicrystalline polymers form lamellae, and these lamellae are organized into lamellar stacks. In uniaxially drawn polymers, especially in fibers, these lamellar stacks may form fibrils. The surface normal of the lamellar crystals could tilt away from the fiber axis as a results of this draw,[1−5] and the position of the lamellae in neighboring fibrils may even be correlated.[5−8] The small-angle scattering (SAS) patterns from such structures are spread onto curves symmetrical about the draw axis. These are often categorized as two-point or four-point patterns, the latter sometimes resembling the butterfly pattern frequently found in light scattering. The position, orientation, and the shape of the small-angle reflections can be analyzed to obtain details of the lamellar organization.

There are two main avenues for analyzing these SAS data. One is to interpret 1-D correlation functions obtained by Fourier transforming the data. Ruland,[9] Vonk,[10] and Strobl[11] and their co-workers have studied isotropic samples in this way. Ruland later proposed an extension of this method to analyze the two-dimensional data from anisotropic samples.[12] Stribeck et al. have recently analyzed the 2-D data from fibers by collapsing the data onto two perpendicular axes.[13,14] The other avenue is to interpret the intensity distribution itself in terms of various models. The Guinier approximation to the one-dimensional particulate scattering is a classic example of this type of analysis.[15] Various types of 1-D models can be refined by fitting the calculated intensity to the data.[16−18] A similar analysis in two dimensions has proved to be quite difficult. An understanding of the structural features that control the form of the 2-D SAS data can be achieved by full parametrization of the data in 2-D. More importantly, this also allows quantitative evaluation of changes in the 2-D data and correlation of these changes to process and performance. We recently showed that elliptical coordinates provide an appropriate framework for analyzing SAS data from oriented polymers.[19−21]

We can now demonstrate that an ellipse provides a best fit to the distribution of the intensities in lamellar reflections and will illustrate the use of the method in practical applications. The analysis will be illustrated using small-angle X-ray scattering (SAXS) data from nylon-6 fibers.[22] It is equally applicable to neutron and light scattering data and to other polymers. We will use the term fiber in our discussion in a broader sense to include uniaxially oriented structures. Extensive modeling trials have shown that small size and misorientation of the lamellar stacks cannot by themselves account for the observed shape of the SAS reflection. Elliptical SAS reflections have been seen in a variety of nonfiber systems[23−25] and assigned to affine deformation of a system that was isotropic before deformation.

Experimental Section

Much of the data used in this paper have been reported in our earlier publications.[19,22] Briefly, SAXS patterns from six spun-drawn fibers and two pairs of drawn-annealed fibers were collected at the Cornell High Energy Synchrotron Source using a wavelength of 0.908 Å and a sample-to-detector (C) of 743 mm. The Fuji image plate system used for data collection had a resolution of 0.1 mm and an image size of 2048 × 2500 pixels. The central region of each image was extracted and adjacent pixels binned together to give a 300 × 300 image with 0.2 mm per pixel. For the original peak fitting, the image was further binned into a 100 × 300 image, and single columns—averaged over 0.6 mm in the equatorial or x direction—were used in the program PeakFit (Jandell). Each of these longitudinal 1-D intensity profiles was fitted by the sum of four modified Lorentzian peaks—two to describe the central diffuse scattering and one each to describe lamellar peaks above and below the equatorial streak. This scheme provided the best fit to the data with least number of parameters.[22] Modified Lorentzians are Pearson VII functions with the power parameter m fixed

† AlliedSignal Inc.
‡ Cornell University.
* Corresponding author. Phone (973) 455-3764; Fax (973) 455-5295; E-mail nsmurthy@alliedsignal.com.

10.1021/ma9911501 CCC: $19.00
Published on Web 01/11/2000

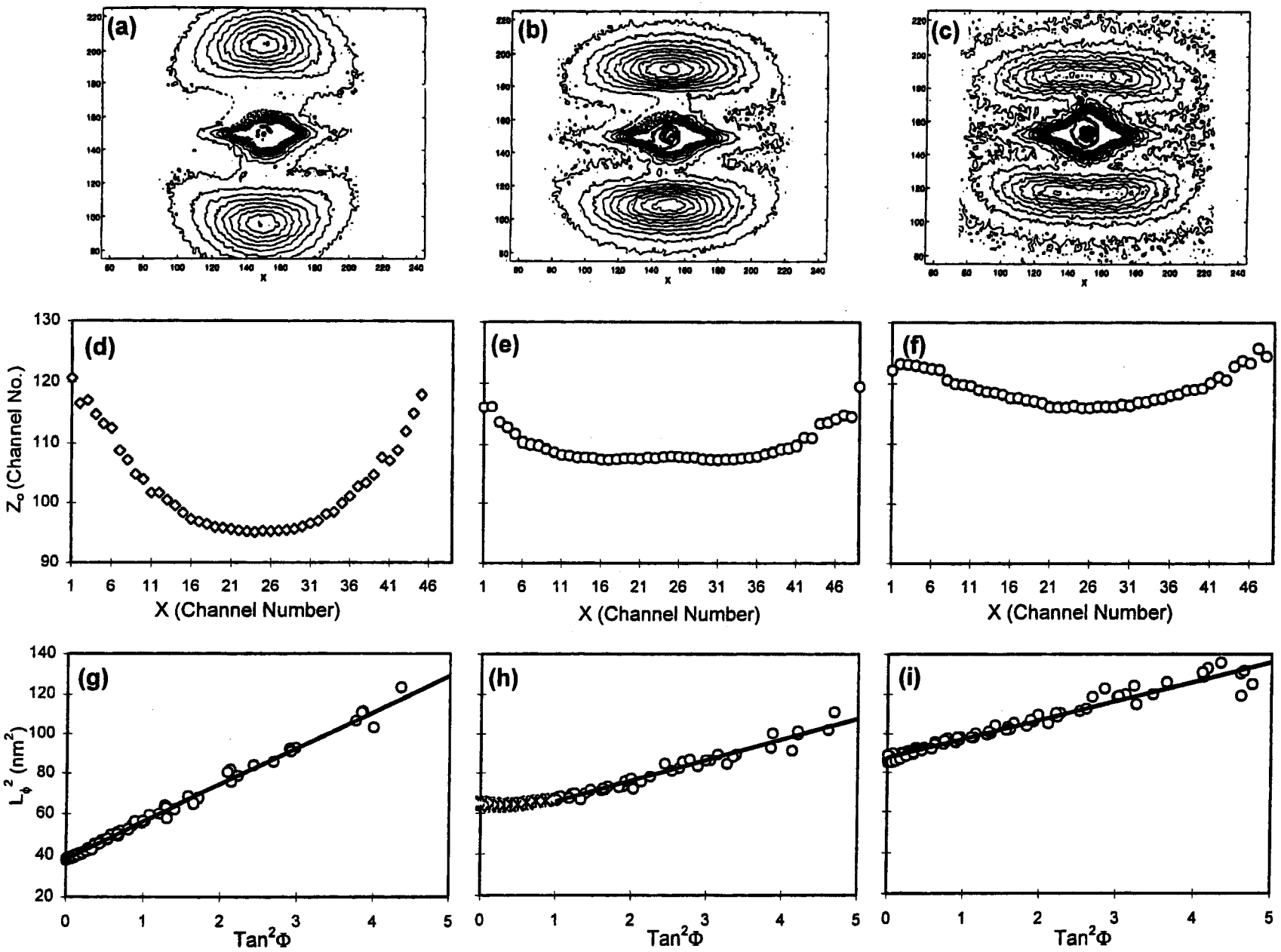

Figure 1. Two-dimensional SAXS pattern from an oriented nylon-6 fiber. These figures show the effect of drawing: left, as-spun; middle, 3.0 drawn; right, 4.5 drawn. Top: 2-D images of the SAXS data. Center: plot of z_0 vs x for the bottom half the 2-D pattern. Bottom: plot of L_ϕ^2 vs $\tan^2 \phi$. There is a cluster of four points at each ϕ value, each corresponding one of the four quadrants.

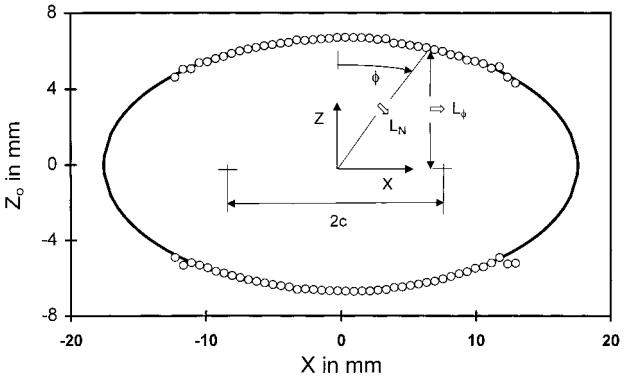

Figure 2. Plot of the lamellar peak position as a function of the distance perpendicular to the fiber axis in a highly drawn and annealed nylon-6 fiber. The elliptical fit to the data is overlaid on the measured data (open circles).

at 2 and have the form

$$I(z) = I(z_0)/[1 + 4(2^{1/m} - 1)\{(z - z_0)/w\}^2]^m \qquad (1)$$

where z_0 is the peak position and w is the full width at half-maximum. z_o is zero for the central diffuse scattering, and the value of z_0 obtained for the lamellar reflections at each value of the lateral position x is used to analyze the contour of the reflection, i.e., locus of the peak maximum.

Data Analysis

Figure 1a−c shows examples of the 2-D SAXS data. In what follows z is the vertical (fiber/meridional) axis and x is the horizontal (lateral/equatorial) axis. The curvature being addressed here is shown in Figure 1d−f, which are plots of the z-coordinate of the peak maximum, z_0, vs x. When it became clear that the best fit for the changes in z_0 as a function of x was an ellipse (Figure 2) or a hyperbola, the data were transformed to give a straight line from these curves. The standard form for an ellipse is

$$(x/a)^2 + (z_0/b)^2 = 1 \qquad (2)$$

For all the data discussed here, $a > b$ so a is the semimajor axis and b the semiminor axis. The magnitude of the scattering vector **s** is $s = 2 \sin \theta/\lambda$, where 2θ is the scattering angle and λ is the wavelength of the radiation, and $s = 1/\text{periodicity}$. Dividing eq 2 by z_0^2, and using $\tan \phi = x/z_0$, where ϕ is the angle between the scattering vector **s** and z, we have

$$(1/z_0)^2 = (1/b)^2 + (1/a)^2 \tan^2 \phi \qquad (3)$$

A plot of $(1/z_0)^2$ vs $\tan^2 \phi$ would be a straight line with a slope of $(1/a)^2$. The intercept of $(1/b)^2$ can be used to calculate the lamellar spacing. The shape of the ellipse can be defined by the distance between the foci, $2c = \sqrt{(a^2 - b^2)}$ or by the dimensionless parameter ellipticity, $\epsilon = (1 - b/a)$.

In the small-angle regime, $2 \sin \theta = \tan(2\theta) = \sqrt{(x^2 + z_0^2)}/C = r/C$, where r is the radial distance from the origin to the point (x, z_0) and C is the distance between sample and detector. In a four-point pattern, let L_N be the lamellar repeat in the direction of the lamellar normal. If r is the distance to this intensity maximum, we have $s = r/(C\lambda) = 1/L_N$; i.e., $(1/r) = (L_N/C\lambda)$. The position of the small-angle reflection on the meridian or fiber (z) axis is widely used to characterize the sample as its "long period" or lamellar repeat distance, L_M. This is true for both "two-point" patterns where the overall intensity maximum is at $\phi = 0$ and for "four-point" patterns where the scattering pattern has well separated off-axis peaks. On the meridian, $x = 0$, $z_0 = + b$ and $s_M = b/(C\lambda) = 1/L_M$; i.e., $(1/b) = (L_M/C\lambda)$. At any arbitrary angle ϕ, let L_ϕ be the periodicity of the lamellar planes measured parallel to z as a function of the angle ϕ that the lamellar reflection makes with the fiber axis (z), and we have $(1/z_o) = (L_\phi/C\lambda)$.

Just as L_M is the periodicity of those lamellae aligned with their normals along the meridian, let L_E be the periodicity (long period) of those lamellae aligned with their normals along the equator. If the intensity of the reflection has fallen to zero before reaching the equator there may be no such lamellae; nevertheless the ellipse intersects the equator at $x = \pm a$, $z_0 = 0$, and $s_E = a/(C\lambda) = 1/L_E$; i.e., $(1/a) = (L_E/C\lambda)$. In terms of these spacings, L_ϕ, L_M, and L_E, eq 3 becomes

$$L_\phi^2 = L_M^2 + L_E^2 \tan^2 \phi \qquad (4)$$

This is a straight line of slope L_E^2 on a plot of L_ϕ^2 vs $\tan^2 \phi$; $\epsilon = (1 - L_E/L_M)$. In the limit where the reflection stays on a straight layer line the intercept on the equator is at infinity, $a = \infty$ ($L_E = 0$) and $b = 0$; the ellipticity is 1. If the reflection follows the arc of a circle, $a = b$, $L_E = L_M$, the ellipticity is zero and $L_\phi = L \sec \phi$. If the slope is negative, then there is no intercept on the equator and no real value of L_E, and the reflection is tracing out a hyperbola with foci on the z-axis. In the standard form for a hyperbola, $-(x/a)^2 + (z_0/b)^2 = 1$. A positive slope and a negative intercept would imply a hyperbola with foci on the x-axis and no real value of L_M. Exactly equivalent plots can be produced in terms of L_N. The ellipse then has the form

$$L_N^2 = L_M^2 - (L_M^2 - L_E^2) \sin^2 \phi \qquad (5)$$

Since our data are in the form of a digital matrix with the fiber axis along the columns, it is easier to measure and use L_M and L_ϕ and so use eq 4.

Examples of the plot of L_ϕ^2 vs $\tan^2 \phi$ are shown in Figure 1g,i. These are excellent straight-line fits out to $\tan^2 \phi = 5$ and $\phi = 66°$. The curvature in Figure 1h will be addressed under "Discussion". The positive slope shows that the tilt of the lamellae is accompanied by an increase in the lattice spacing. The standard deviations of such fits is typically 0.01 nm for long spacing calculated from the intercept ($L_M \sim 10$ nm), 0.03 nm for the slope ($L_E \sim 4$ nm), and 0.003 for ellipticity calculated from the slope and the intercept ($\epsilon \sim 0.6$). We have carried out this analysis on fibers under a variety of drawing and annealing conditions as well as with different polymers. Similar plots obtained with data from other fibers such as PET were recently published.[26]

Although these are excellent fits, they do not by themselves ensure that the formula chosen is the best one. Data were fitted with various polynomial expansions in ϕ and in $\tan(\phi)$. These showed that the asymmetry was very small, with coefficients of odd terms at least 2 orders of magnitude smaller than those of even terms. Even expansions in $\tan(\phi)$ gave results such as $y^2 = 44.451 - 0.1576x^2 + 9 \times 10^{-5}x^4$, supporting truncation at the second order. Coefficients in even expansions in ϕ varied widely with the number of terms

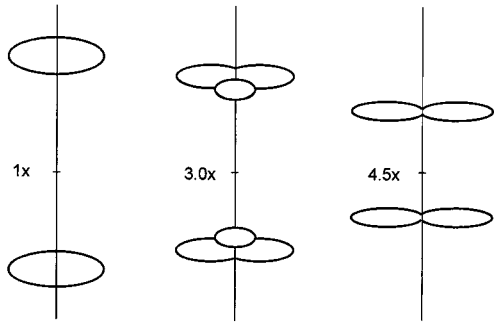

Figure 3. Illustration of the coexistence of two populations of lamellae in moderately drawn fibers. 1x is the as-spun fiber appearing as a two-point pattern, and 4.5x drawn fiber has the four-point pattern. The 3.0x drawn is a composite of the two- and four-point patterns.

and the range of data included, reflecting the slow convergence of the series expansion of $\tan^2 \phi$.

Results

Effect of Drawing. Figure 1a−c shows SAXS data from as-spun, 3.0 drawn, and 4.5 drawn fibers. The data obtained from as-spun fiber are usually described as a two-point pattern and that from the fully drawn fiber as a four-point pattern. Both of these can be described by a single reflection, and the plot of L_ϕ^2 vs $\tan^2 \phi$ is a straight line (Figure 1g,i). The intermediate fiber, the fiber 3.0 drawn, shows a different behavior. The plot of L_ϕ^2 vs $\tan^2 \phi$ deviates from the straight line near the meridian (Figure 1h). This deviation is also apparent in the plot of z_0 vs x in Figure 1e and is due to the presence of two overlapping lamellar reflections as illustrated in Figure 3. The reflection close to the meridian with a long spacing of 8 nm is weak and is a remnant of the as-spun fiber (a two-point pattern), and the outer parts of the reflection at 7.4 nm continue to transform into a four-point pattern. This and other examples that follow show that the L_ϕ^2 vs $\tan^2 \phi$ plot can measure differences as small as 1% in the average value even when the lamellar peaks are quite broad.

Figure 4 shows the variation of various structural parameters as a function of draw ratio. The long period L_M (Figure 4a), the ellipticity ϵ (Figure 4b), and the angular position ϕ_0 of the reflection peak (Figure 4c) are derived from the lamellar SAXS reflection. The diameter d of the lamellar stacks (Figure 4d) is derived by Guinier analysis of the lamellar reflection,[22,27] and the degree of crystalline orientation (Figure 4e) is measured by WAXD.[28] In the plot of long spacing, the squares are four-point reflections and the crosses two-point reflections. As the fiber is drawn, there is an overlap of two- and four-point patterns, indicating the presence of two distinct populations of lamellae. In our earlier analysis we used just one lamellar reflection and found that ϵ reaches a maximum at a draw ratio of 3.0 and then begins to decrease.[19] We now see that the fibers at intermediate draw ratio have two populations of lamellae, and with the two overlapping lamellar peaks separated ϵ does not decrease at higher draw ratios (Figure 4b). The influence of this second lamellar peak is greater in 3 times drawn fiber (Figure 1e) than in the other fibers, and this accounts for the maximum we reported in our earlier paper. At draw ratios >3.5, the structure is dominated by the four-point pattern with a single long spacing.

The ellipticity and angular positions are taken from the stronger reflection, which is a four-point pattern. In the case of the as-spun fiber, draw ratio 1, the fitting routines find a small angular separation and thus a four-point pattern, but to the eye it appears to be a two-point pattern and is usually described in that way. The solid lines in all of the plots in Figure 4 are fits based on semiaffine deformation of the lamellar stacks. This is an affine deformation with an extension ratio less than that of the macroscopic fiber but proportional to it. Figure 4f shows that the internal effective extension ratio λ_{SAXS} calculated from the SAXS ellipticity, λ_{SAXS}^3

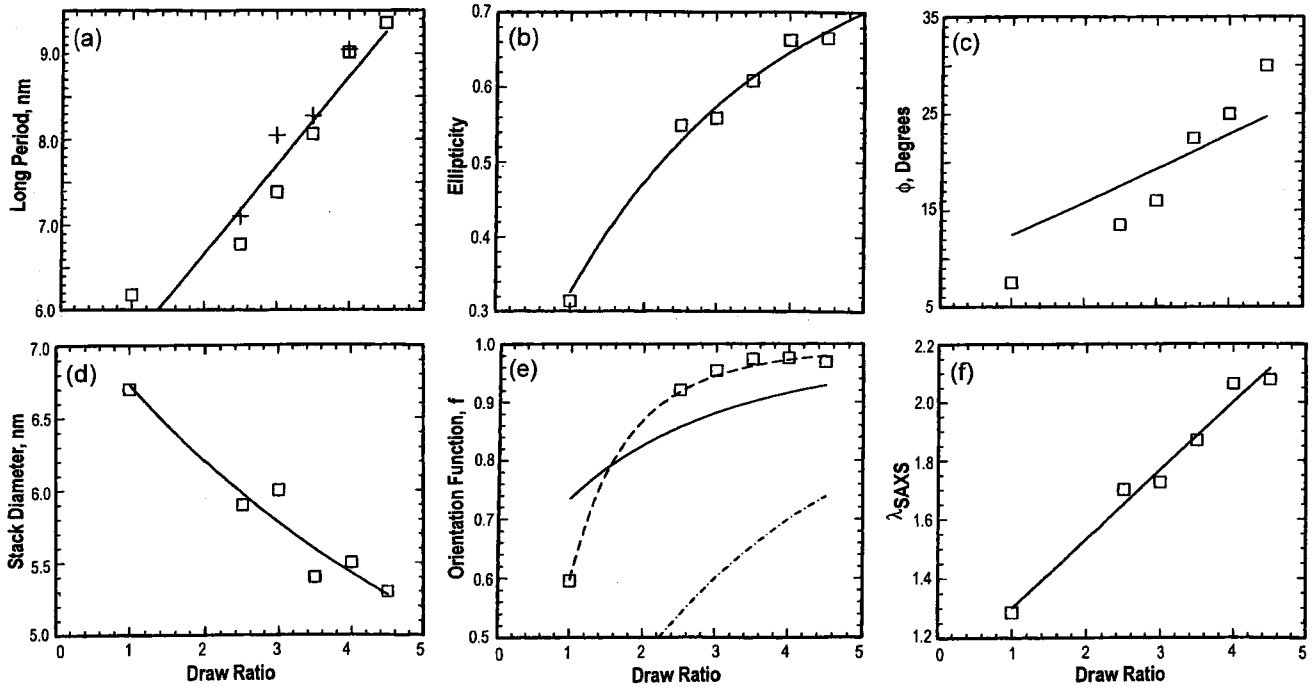

Figure 4. Change with draw ratio of (a) long spacing, (b) ellipticity, (c) angle between the peak of the lamellar reflection and the fiber axis, (d) lamellar stack diameter, (e) degree of crystalline orientation, and (f) the extension ration λ as calculated from SAXS ellipticity. The lines through the observed points are the fits to affine transformation.

$= (a/b)^2$, is indeed a linear function of the external draw ratio R, i.e., $\lambda_{SAXS} = mR + c$, where the intercept c is 1.06 and the slope m is 0.23. This relation converts external draw ratio R into the internal effective draw ratio λ_{SAXS} in obtaining the fits for other plots: $L = \lambda_{SAXS} L_0$ in Figure 4a, $\epsilon = 1 - \lambda_{SAXS}^{-3/2}$ in Figure 4b, $\phi = 2 \tan^{-1} (\lambda_{SAXS}^{3/2} \tan \phi_0)$ in Figure 4c, and $d = d_0/\sqrt{\lambda_{SAXS}}$ in Figure 4d. (ϕ_0 and d_0 are the azimuthal angle between the reflections and the stack diameter, respectively, in the as-spun fiber.) In Figure 4e for the crystal orientation, the bottom dot−dashed curve is the affine fit to the Hermans orientation function ($f = 3 \langle \cos^2 \phi \rangle - 1)/2$; ϕ is related to the draw ratio as in Figure 4c but here refers to the azimuthal angle in the WAXD data). The disagreement between the crystal orientation predicted from SAXS and that measured by WAXD shows that the relation between deformations of the lamellar stacks and the crystals within the lamellae cannot be described by a simple model (see "Discussion").

Effect of Annealing. Parts a and b of Figure 5 show the data for highly drawn and moderately drawn fibers, respectively, before and after annealing. The expected increase in the lamellar spacing upon annealing is seen as an increase in the intercept. More interesting is the observation that the plots in the unannealed fibers are a composite of two populations with different lamellar spacings: one a two-point pattern on the meridian (shown as triangles) and the other a four-point pattern (shown as squares). The lamellar spacing and the ellipticity of the two populations in the unannealed fibers are calculated by least-squares fitting the two segments to straight lines as shown in Figure 5. This shows that the ellipticities of the two populations are the same. Only one population is present in the annealed fibers, and the ellipticity does not change upon annealing.

Skin−Core Effect. There is a distribution in lamellar spacing in all fibers that contributes to the meridional width of the lamellar reflections. Our data (Figures 1a, e, h, and 5; illustrated in Figure 3) show that fibers may also have two distinct populations of lamellae. The populations are distinguished by means of 2-D information; it would be very difficult to determine that there were distinct groups using only the long spacing distribution. A spread in lamellar spacing could be due to local fluctuations in spinning speed, draw ratio, or temperature of draw. However, the presence of two distinct populations is most likely due to the large difference between the skin and the core of the fibers. The skin is quenched more rapidly and experiences higher shear forces than the core, which cools more slowly and is able to flow. These differences are known to disappear on extensive drawing or annealing, conditions that make the two populations we see become one. Accepting this, the analysis described here allows us to study the skin/core structure by bulk diffraction measurements—less direct but less difficult than microdiffraction.

Mechanisms such as melting and recrystallization, commonly invoked to explain the increase in the crystallite size and crystalline perfection upon annealing, may explain the conversion of two populations into a single one. It is possible that relatively unchanged "as-spun" fiber is present in the core of the fiber, and the fraction that gives rise to the four-point pattern first appears near the skin and propagates toward the core. A difficulty with this interpretation is that drawing tends to increase L (Figure 4a), but the "original" two-point pattern has a larger long spacing than the "drawn" four-point pattern when both are present. It appears from Figure 4a that although drawing increases L, the transformation from two-point to four-point reduces this effect.

Further Data Analysis

The data analysis described above used 1-D sequential fitting of vertical slices from the 2-D pattern. A full 2-D analysis seems more natural, and it is indeed possible to get very good fits for the full SAS pattern using only a few parameters in elliptical coordinates.[19−21] However, suitable functional forms must be assumed. Each mathematical assumption made for convenience is equivalent to a structural model assumption that may not be so acceptable. For example, the analysis has been based on the assumption that the intensity can be expressed as a product of two orthogonal functions $f(u)$ and $g(v)$ in a (u,v) coordinate system. This is equivalent to assuming that there are independent distributions of lamellar properties—that the perfection and size of lamellar stacks are independent of the stack orientation. Using this simple assumption, we can fully account for the curvature of the position of the peak maximum. However, the model predicts that the peak widths for slices taken parallel to the z-axis should be fairly constant, while the widths of the peaks for the real data start to *increase* when the slices are far enough from the z-axis (Figure 6). This discrepancy causes a poor fit of the whole 2-D pattern.

In earlier work where the SAXS pattern was analyzed in Cartesian coordinates, we showed that a Gaussian distribution of orientations of the lamellar stack accounts for this increase in width along the z-axis.[22] This applied to lamellar reflections the method previously used to analyze the equatorial streak.[29,30] Unknown to us, an analysis of the effect of misorientation on continuous layer lines in WAXD had already predicted similar effects.[31,32] To combine misorientation and the elliptical coordinate system, the rotationally smeared intensity $J(u,v)$ is calculated as

$$J(u,v) = \int_{-90}^{90} I(u',v') \exp\left(-4 \ln(2) \frac{\Psi^2}{w_\Psi^2}\right) d\Psi \quad (6)$$

Here Ψ is the angle a particular ellipse defined by (u',v') makes with the x-axis, and w_Ψ is the full width at half-maximum of the Gaussian distribution. The rotated elliptical coordinates u' and v' are calculated by first obtaining a rotated Cartesian system, x', z' as

$$x' = (x - x_c) \cos(\Psi) + (y - y_c) \sin(\Psi)$$
$$z' = (z - z_c) \cos(\Psi) - (x - x_c) \sin(\Psi) \quad (7)$$

where (x_c,z_c) is the center of the pattern and (x,z) are the actual $x-z$ coordinates. Then the standard equations for elliptical coordinates are applied:

$$x' = (u'^2 + (2c)^2)^{1/2} \cos(v')$$
$$y' = u' \sin(v') \quad (8)$$

As before, the intensities are expressed as a product of two modified Lorentzian functions $f(u)$ and $g(v)$[19] but

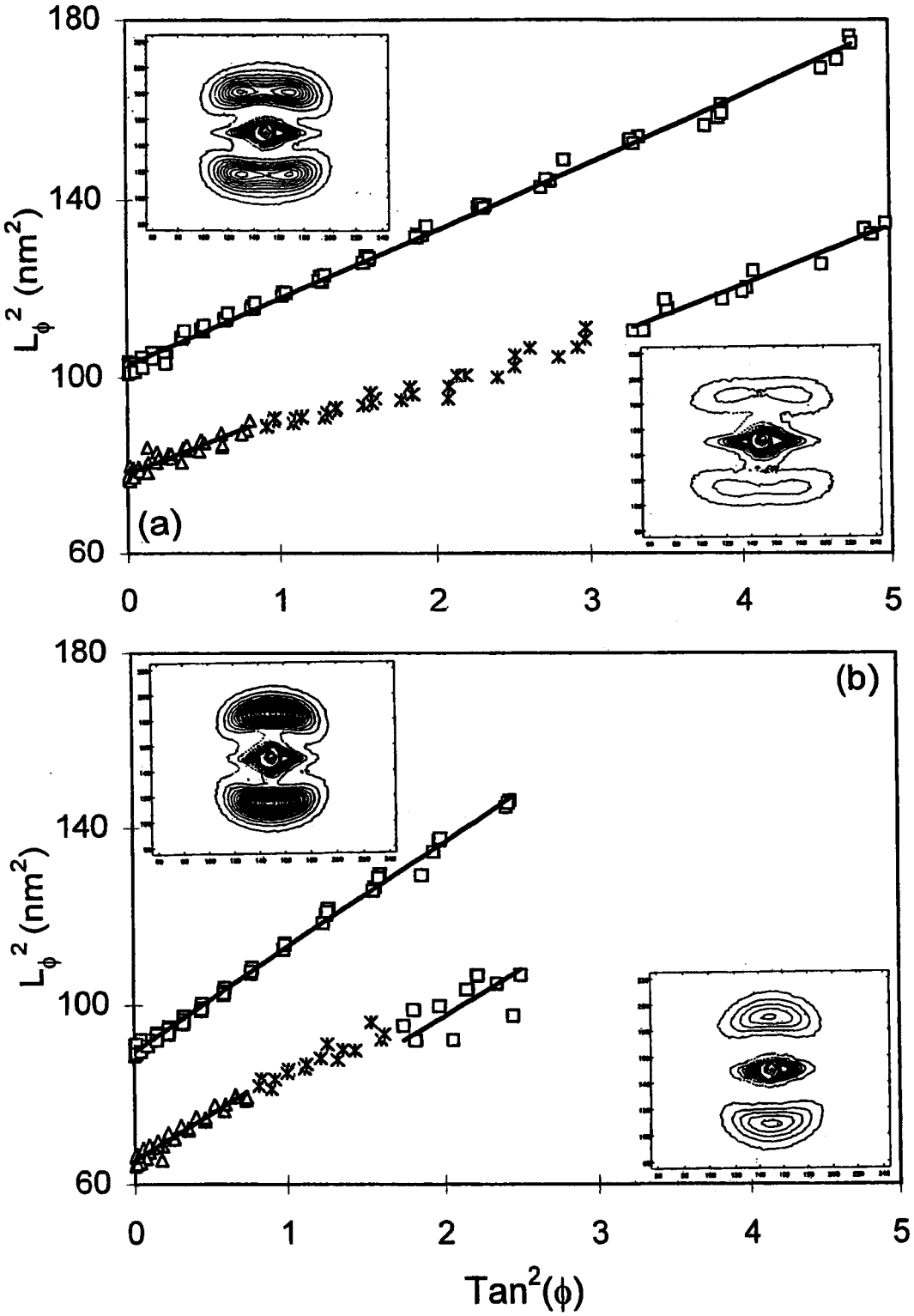

Figure 5. Effect of annealing: (a) highly drawn fiber; (b) moderately drawn fiber. The bottom curve in each figure is the spun-drawn fiber, and the top curve is the annealed fiber.

now in the rotated elliptical (u',v') coordinate system.

$$I(u',v') = I(0,0)\, f(u')\, g(v') \tag{9}$$

In practice, the angle Ψ is replaced in all formulas by $(\Psi - \Psi_0)$ to allow for misalignment of the fiber axis from the vertical. The misalignment Ψ_0 is refined during the least-squares fitting. Figure 6 shows the peak width (measured along z) as a function of distance from the meridian for the data shown in Figures 2 and 5a (annealed). A value of 24° for w_Ψ produces almost the observed width increase while the fit of peak position is maintained. This shows that misorientation combined with an elliptical fit can account for all the observed features in the intensity distribution in the lamellar reflections. Considered simply in terms of curve fitting, we have improved the fit considerably with one extra parameter, w_Ψ. A similar improvement could be made by explicitly having the width of the reflection in u be a linear function of v. In this case the intensity is no

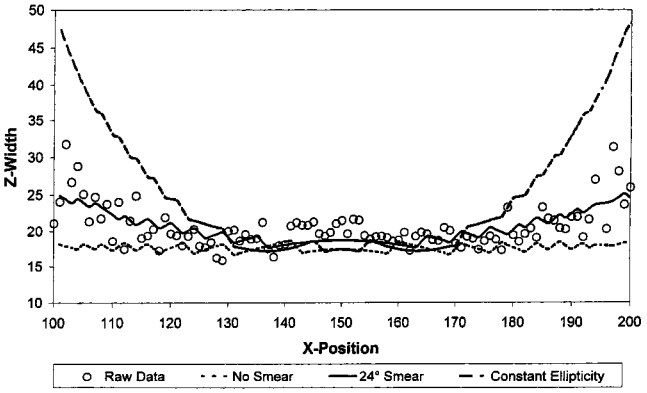

Figure 6. Generation of the increase in the width of the lamellar reflections with x by using an average 24° tilt of the elliptical coordinate system.

longer a product of functions $f(u)$ and $g(v)$, and the structural implication is that rotated stacks have a shorter coherence length.

Also shown in the figure is the change in the width of the lamellar peak if the data were fitted to a constant a/b ratio rather than a constant distance $2c$ between the two foci, the method that we used in our earlier publication.[19] The fit with constant $2c$ requires that the misorientation factor be taken in to account to explain the increase in the z width of the lamellar peak with x. In marked contrast, the fit constant a/b generates far too much increase in z width even without any misorientation. Thus, an elliptical coordinate system with constant $2c$, along with misorientation of the lamellar stacks, provides the most appropriate framework for fitting the SAS data.

Discussion

To summarize the results, we find that the lamellar reflection from fibers is best fitted by an elliptical form. When the reflection does not fit an ellipse, we can get more meaningful results by assuming that there are two superposed reflections, each elliptical. Description of the data is then easier when elliptical coordinates (u,v) are used. The major features of the pattern can be fitted by an intensity $I(u,v)$ expressed as a product of two functions, $f(u)$ and $g(v)$. But in this case, to fit details such as the width of the weaker regions of the pattern, we must add rotational disorder to the model. The model implies that there exists a specific correlation between lamellar tilt and lamellar period that gives the ellipse and then that the entire structure is subject to misorientation, every element to the same extent. This simplification adds rotational disorder to the fit with only one additional parameter.

There are two important questions: (1) Can a combination of rotational disorder and limited lateral size produce an elliptical reflection? (2) What microstructures can yield the elliptical form, and how could they be formed during deformation?

It is helpful to begin by considering the diffraction expected from a range of possible structures. An ideal structure is perfectly aligned and has a large lateral coherence. It may be considered as a convolution of a 1-D lattice, spacing L_M, aligned along the fiber axis and a surface discontinuity. In general, this discontinuity is oblique, as shown in Figure 7a. It may be interpreted as the surface of a single tilted lamellar crystal, [1−4] as the locus of the surface of several smaller crystals that

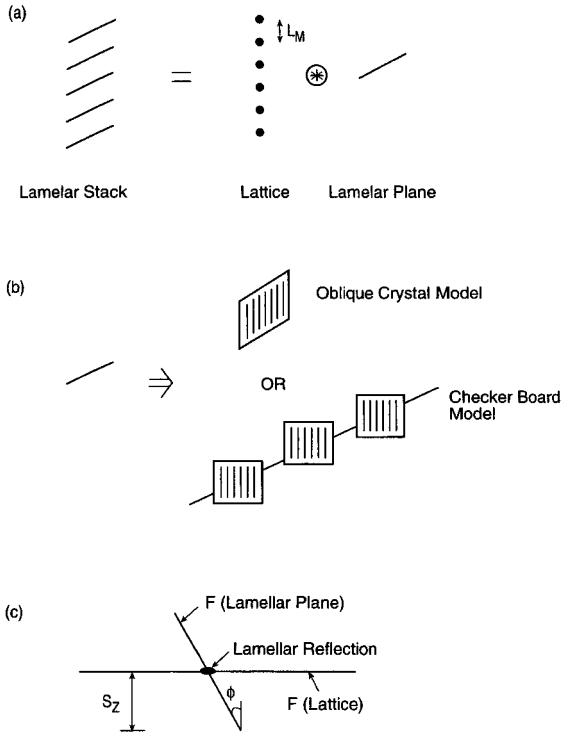

Figure 7. Illustration of origin of SAS profiles: (a) lamellar structure viewed as the convolution of one-dimensional lattice and a lamella; (b) two explanations for the origin of the lamellar tilt; (c) lamellar reflection as a product of the Fourier transform of the two components in (a).

belong to neighboring stacks or fibrils,[5−7] or as a combination of these.[8] Both models are shown in Figure 7b, and the present analysis is applicable to both models, although discussion here is given in terms of lamellae. The diffraction pattern from such an idealized structure is the product of the Fourier transforms of the two real space elements. The Fourier transform of the one-dimensional lattice is a set of horizontal lines, spacing $1/L_M$; that of the single oblique discontinuity is a line normal to the lamellar plane. The product of these two is a set of points lying on this line (Figure 7c). Imperfections in the real system weaken and spread all but the first-order points. Thus, the diffraction pattern is a pair of off-axis points. This gives four points in a fiber diffraction pattern, since symmetry requires surfaces of opposite obliquity, unless the lamellae are oriented perpendicular to the fiber axis, when there will be two points on the meridian.

If there is misorientation—a distribution of body rotations of the whole structure—then the typical point is smeared into an arc of a circle. If the crystal width is small, then the ideal lamellar structure is multiplied by a horizontal limiting function. The effect in the diffraction pattern is that the points are convoluted with a horizontal spread function, the Fourier transform of the limiting function. Thus, rotational disorder of a lamellar stack produces a circular arc, and limited lateral size gives a straight layer line. Both imperfections are always expected to be present in oriented polymers. Since the observed elliptical traces lie between these extremes, it is natural to think that some combination of the two might be the cause. This has been tested (a) by smearing trial functions to attempt to produce the form of the data and (b) by desmearing the data to attempt to produce a flat layer line.

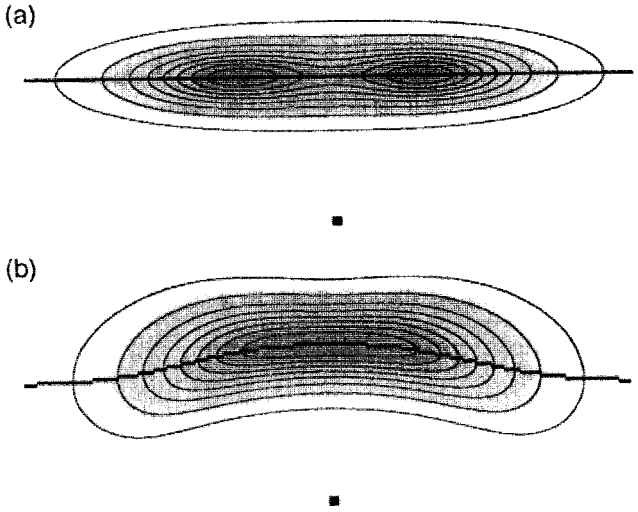

Figure 8. Curvature in z_0 vs x produced by desmearing due to misorientation. Synthetic data in which the peak maximum occurs at a constant z_0 are shown in (a), and these data are rotationally smeared with a Gaussian half-width of 25° in (b).

First, simulated data were rotationally smeared to see whether an elliptical shape could be produced from the starting point of a straight layer line, that is, from an intensity $I(x,z) = I(0,0)\ F(x)\ G(z)$. Direct numerical computation was used to determine an integral similar to that in eq 6 but using x, z, and Ψ. Pearson VII functions were used for $F(x)$ and $G(z)$, while the rotational disorder was Gaussian. It was found that the position of the peak intensity, z_0, could approximate to an ellipse for small distances from the center line, but no combination could be found where the slope of z_0 versus x continues to increase as in Figures 1g−i and Figure 5. Instead, the maximum position tends to flatten out. Figure 8a shows the original (synthetic) data, with the peak position z_0 = constant. Figure 8b is the same data rotationally smeared with a Gaussian of half-width 25° (comparable to that required in the elliptical model). It is clear that the maxima are not near to following an ellipse.

To extend the range of trial functions, a "round spot" with modified Lorentzian distributions was tried, with the general form of $I(x,z) = I(0,0)/[1 + (x/w_x)^2 + (z/w_z)^2]^2$. The results were essentially unchanged. The problem with all approaches of this type is that a specific functional form of the original intensity must be chosen; one cannot prove that there is no other form that would have better properties.

A more direct method is to rotationally deconvolute the data and see what the resulting "original" intensity distribution would be. Data are transformed from (x,z) to (r,θ), Fourier transformed in θ, filtered, divided by a Gaussian, inverse transformed, and finally returned to Cartesian coordinates. Because of the difficulty of filtering noise without distorting the data, unfiltered synthetic data sets were used initially. The experimental data were fitted as described in the data analysis section, and the elliptical fitting parameters were used to create a noise-free data set that included a Gaussian misorientation. Figure 9a shows the typical elliptical form of the peak positions, and Figure 9b shows the increase in the width of the lamellar peak with s_x. Rotationally deconvolving the data, we see that position still follows the elliptical shape (Figure 9c) whereas the width of the peak is now constant over most of the data range (Figure 9d).

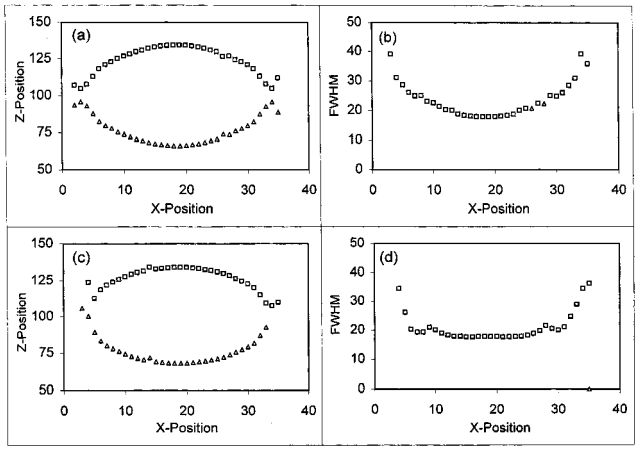

Figure 9. Effect of deconvolution on an "ideal" experimental pattern in which the (a) the lamellar peak position falls on an elliptical curve and (b) the z width of the lamellar increase with x. Effect of deconvolution for the misorientation on (a) the position and (b) the width.

Deconvolution of real data is difficult when the equatorial streak is strong. A single pattern from a wet nylon-6 fiber that has essentially no equatorial streak was used for this test. The basic result was that the deconvoluted pattern broke up into strong oscillations of intensity before a flat layer line was reached. Increasing the amount of filtering makes the initial pattern more circular so that even with a greater amount of desmearing, the flat layer line is not achieved. No way has been found to make misorientation completely account for the elliptical position of the lamellar peak.

We can now proceed to the second question posed above: what structures can produce the observed elliptical shape, and how might they be formed? Since rotation of lamellae of the same long period cannot produce the observed structure, the requirement is a correlation between the L_ϕ and ϕ. If lamellae deform by chain slip, their surfaces rotate while the lattice along the fiber axis is unchanged. Using Venetian blinds as an analogy makes this clear. Opening and closing a Venetian blind by rotating the slats leaves the vertical separation of the slats unchanged. However, the separation of the slats in the direction normal to their surfaces decreases with tilt. Here L_M = constant or $L_\phi \propto \cos\phi$, and the result is that the reflection moves along a horizontal layer line. This is shown in Figure 10a. In the oblique crystal model (Figure 7b) fibrillar slip would have the same effect. If the rotation of the lamellar planes is associated with a change in the 1-D lattice spacing (measured along the fiber axis), then the locus of the reflection is no longer a straight line. An increase of the lattice spacing as the lamellar surfaces rotate away from perpendicular to the fiber axis produces a line with negative curvature; a decrease in the lattice spacing and the same rotation produces a line with positive curvature. Both cases are shown in Figure 10.

A simple mode of deformation that produces the correct combination of shear and interface rotation is affine deformation. Any circular pattern in small-angle scattering will change to an ellipse after the material undergoes affine deformation. Brandt and Ruland[25] demonstrate this in quite general terms. The material they studied is a styrene−isoprene−styrene block copolymer with styrene spheres of about 20 nm in diameter that form bcc microdomain structures. After deformation the SAXS patterns are elliptical, and they

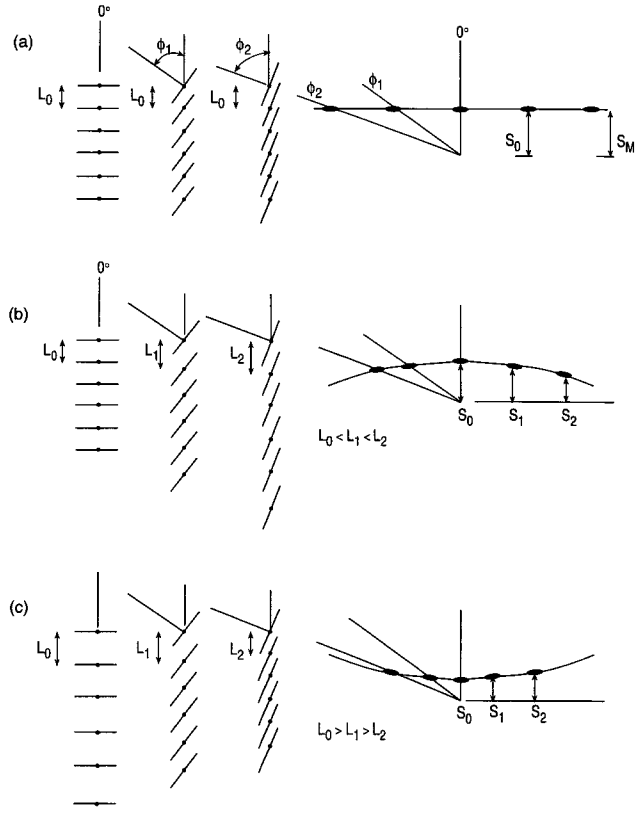

Figure 10. (a) A straight trace resulting from the tilting of the lamellae with no change in the lattice spacing. (b) An elliptical trace due to the expansion of the lattice with the tilting of the lamellae. (c) A hyperbolic trace as a result of the contraction of the lattice with the titling of the lamellae.

were analyzed by plotting z_0^2 vs x^2, i.e., using eq 2 that we independently rediscovered while analyzing our data. For a uniaxial extension ratio λ it is easy to see that periodicity along the draw direction is increased by a factor λ, while at constant volume periodicities perpendicular to the draw direction are reduced by $(1/\sqrt{\lambda})$. Thus, ellipticity $= (1 - \lambda^{-3/2})$ and the effective draw ratio derived from the SAXS pattern, $\lambda_{SAXS} = (1 - \epsilon)^{-2/3}$, i.e., $\lambda_{SAXS}{}^3 = (a/b)^2$ in reciprocal space or $\lambda_{SAXS}{}^3 = (L_M/L_E)^2$ in real space. In the case of this block copolymer, $\lambda_{SAXS} = \lambda$ at least up to $\lambda = 2.5$, the highest value measured.

In our case, although there is a linear relation between λ_{SAXS} and λ, λ_{SAXS} is always smaller. The relation is best described by a strain in the stack that is 0.233 of the fiber strain, while the stack strain in the as-spun fiber is 0.3. Figure 4f shows this relationship. A lower stack strain may be expected because the stacks contain rigid crystals, and amorphous deformation can occur outside the stacks. An affine deformation predicts that L_M is proportional to draw ratio, and the fit in Figure 4a is a line corresponding to the expression $L = \lambda_{SAXS} L_0$, where L_0 is the long spacing in the unstrained lamellar stack. The fit is good, although it appears that the initial redraw is different from further drawing. The ellipticity plot in Figure 4b contains the same information as Figure 4f and shows that, in this view, the initial redraw is no different from the further drawing. The fit to the angle of peak intensity, in Figure 4c, shows an approximate agreement with the predictions of affine deformation, but the angle changes more rapidly than predicted. However, the peak intensity tracks the angle where there are the most well organized stacks, and any reorganization will affect the data. Even for the block copolymer, detailed considerations of distortion were required to fit the angular intensity profile.[25] The decrease in the stack diameter (Figure 4d) is well modeled as $(A/\sqrt{\lambda_{SAXS}})$ as predicted by affine deformation. However, the crystalline orientation (Figure 4e) is not in agreement with the simple model. Using λ_{SAXS} as the deformation of an isotropic material gives the low orientation indicated by the dashed line well below the data. We must allow that the high-temperature deformation that produced the as-spun fiber has oriented the crystals while allowing the stacks to relax. Putting the effective draw ratio of the as-spun fiber to 2 gives the solid line, which still predicts too little effect on drawing. The dashed line through the data is obtained by allowing the fractional strain to increase from 0.233 to 0.6.

It is not surprising that there are discrepancies with the affine predictions. Any fiber drawing process, particularly at elevated temperatures, is thought to involve reorganization as well as deformation. Local melting and recrystallization may reduce the mean stack deformation by relaxing the loads. Thus, the apparent strain for crystal orientation may be larger because the stack stain is partially relaxed. However, on annealing the long period changes while the SAXS ellipticity remains constant. It appears that in this case melting and recrystallization occur within the steric and spatial constraints of the preexisting structures. Even when part of an increase in L_M on drawing is due to replacement of lamellar stacks with those of larger long period, an elliptical form may be maintained.

Conclusions

2-D SAS data from oriented fiber structures can be fully parametrized in elliptical coordinates. Incorporating the effect of misorientation further refines this approach. The data show that in some fibers there can be more than one lamellar system. This appears as an overlapping of two- and four-point diffraction patterns and is attributed to the skin−core morphology in fibers. Affine deformation can account for the elliptical form of the intensity distribution. It can also account for changes in other structural features on deformation, even though the lamellar stacks deform less than the fiber, and mechanical anisotropy is ignored. While 1-D projections give numerical information on the structure in the direction of the projection axis, it seems that they are best used when the intensity is well concentrated at some orientation or on some layer line. Elliptical fits are better when orientation and its distribution cannot be ignored.

References and Notes

(1) Pope, D.; Keller, A. *J. Polym. Sci., Polym. Phys. Ed.* **1975**, *13*, 533.
(2) Young, R. J.; Bowden, P. B.; Ritchie, J. R.; Rider, J. G. *J. Mater. Sci.* **1973**, *8*, 23.
(3) Matyi, R. J.; Crist, B., Jr. *J. Mater. Sci.* **1978**, *16*, 1329.
(4) Gilman, T. H.; Resetaritis, M. R; Crist, B., Jr. *Polym. Sci. Eng.* **1978**, *18*, 477.
(5) Zheng, Z.; Nojima, S.; Yamane, T.; Ashida, T. *Macromolecules* **1989**, *22*, 4362.
(6) Statton, W. O. *J. Polym. Sci.* **1959**, *41*, 143.
(7) Hosemann, R. *J. Polym. Sci. C* **1967**, *20*, 1.
(8) Vonk, C. G. *Colloid Polym. Sci.* **1979**, *257*, 1021.
(9) Ruland, W. *Colloid Polym. Sci.* **1977**, *255*, 417.
(10) Vonk, C. G.; Kortleve, G. *Kolloid Z. Z. Polym.* **1967**, *220*, 19.
(11) Strobl, G. R.; Schneider, M. *J. Polym. Sci., Polym. Phys. Ed.* **1980**, *18*, 1343.
(12) Ruland, W. *Colloid Polym. Sci.* **1978**, *256*, 932.

(13) Stribeck, N. *J. Polym. Sci., Part B: Polym. Phys.* **1999**, *37*, 975.
(14) Stribeck, N.; Fakirov, S.; Sapoundjieva, D. *Macromolecules* **1999**, *32*, 3368.
(15) Guinier, A. *X-Ray Diffraction*; John Wiley: New York, 1963, pp 319−333.
(16) Murthy, N. S.; Akkapeddi, M. K.; Orts, W. J. *Macromolecules* **1998**, *31*, 142.
(17) Murthy, N. S.; Wang, Z.-G.; Hsiao, B. S. *Macromolecules* **1999**, *32*, 5594.
(18) Jenkins, P. J.; Donald, A. M. *Polymer* **1996**, *37*, 5559.
(19) Murthy, N. S.; Zero, K.; Grubb, D. T. *Polymer* **1997,** *38*, 1021.
(20) Murthy, N. S.; Grubb, D. T.; Zero, K. *Proc. ACS Div. Polym. Mater.: Sci. Eng.* **Aug 1998**, *79*, 363.
(21) Murthy, N. S.; Grubb, D. T.; Zero, K. In *ACS Symposium Series on Scattering from Polymers;* Hsiao, B. S., Lohse, D. J., Cebe, P., Eds.; American Chemical Society: Washington, DC, 1999.
(22) Murthy, N. S.; Bednarczyk, C.; Moore, R. A. F.; Grubb, D. T. *J. Polym. Sci., Polym. Phys.* **1996**, *34*, 821.
(23) Young, P.; Stein, R. S.; Kyu, T.; Lin, J. S. *J. Polym. Sci., Part B: Polym. Phys.* **1990**, *28*, 1791−1812.
(24) Russell, T. P.; Brown, H. R.; Grubb, D. T. *J. Polym. Sci., Polym. Phys.* **1987**, *25*, 1129.
(25) Brandt, M.; Ruland, W. *Acta Polym.* **1996**, *47*, 498.
(26) Murthy, N. S.; Grubb, D. T.; Zero, K.; Nelson, C. J.; Chen, G. *J. Appl. Polym. Sci.* **1998**, *70*, 2527.
(27) Crist, B., Jr. *J. Appl. Crystallogr.* **1979**, *12*, 27.
(28) Murthy, N. S.; Bray, R. G.; Correale, S. T.; Moore, R. A. F. *Polymer* **1995**, *36*, 3863.
(29) Ruland, W. *J. Polym. Sci., Part C* **1969**, *28*, 143.
(30) Grubb, D. T.; Prasad, K. *Macromolecules* **1992**, *25*, 4575.
(31) Holmes, K. C.; Leigh, J. B. *Acta Crystallogr.* **1974**, *A30*, 635.
(32) Stubbs, G. J. *Acta Crystallogr.* **1974**, *A30*, 639.

MA9911501